Premixed flames for arbitrary combinations of strain and curvature

H. Böttler[a,*], A. Scholtissek[a], X. Chen[b], Z. Chen[b], C. Hasse[a]

[a] *Institute for Simulation of reactive Thermo-Fluid Systems, TU Darmstadt, Otto-Berndt-Straße 2, 64287 Darmstadt, Germany*
[b] *SKLTCS, CAPT, BIC-ESAT, Department of Mechanics and Engineering Science, College of Engineering, Peking University, Beijing 100871, China*

Abstract

Many modeling strategies for combustion rely on laminar flamelet concepts to determine structure and properties of multi-dimensional and turbulent flames. Using flamelet tabulation strategies, the user anticipates certain aspects of the combustion process prior to the simulation and selects a flamelet model which mimics local flame conditions in the more complex configuration. Flame stretch, which can be decomposed into contributions from strain and curvature, is one of the conditions influencing a flame's properties, structure, and stability. The objective of this work is to study premixed flame structures in the strain-curvature space using a recently published composition space model (CSM) and three physical space models for canonical flame configurations (stagnation flame, spherical expanding flame and inwardly propagating flame). Flames with effective Lewis numbers both smaller and larger than unity are considered. For canonical laminar flames, the stretch components are inherently determined through boundary conditions and their specific flame configuration. Therefore, canonical flames can only represent a certain sub-set of stretch effects experienced by multi-dimensional and turbulent flames. On the contrary, the CSM allows arbitrary combinations of strain and curvature to be prescribed for premixed flames exceeding the conditions attainable with the canonical flame setups. Thereby, also influences of negative strain effects and large curvatures can be studied. A parameter variation with the CSM shows that flame structures still significantly change outside the region of the canonical flame configurations. Furthermore, limits in the strain-curvature space are discussed. The present paper highlights advantages of composition space modeling which is achieved by detaching the representation of the flame structure from a specific canonical flame configuration in physical space.

Keywords: premixed flames, composition space, stretch effects, negative strain, curvature

*Corresponding author:
Email address: boettler@stfs.tu-darmstadt.de (H. Böttler)

1. Introduction

CFD simulations with flamelet-based chemistry tabulation, as utilized in flamelet-generated manifolds (FGM) [1] or flame-prolongiation of ILDM (FPI) [2], rely on the assumption that a turbulent flame can be considered a statistical ensemble of one-dimensional laminar flamelets [3]. These flamelets can be computed prior to the combustion simulation and tabulated as a function of a reduced set of scalars. During simulation runtime, thermochemical quantities and source terms are obtained from the table instead of computing them in every cell and time step. The application of the approach requires the user to anticipate certain aspects of the combustion process prior to the simulation and select a flamelet model which mimics local conditions for the turbulent flame as best as possible.

It is well-established, e.g. from studies of laminar and turbulent fully resolved numerical simulations, that flame physics are significantly affected by flame stretch, flame-wall interactions, multiple fuel streams, or multiphase characteristics, among others. These effects potentially have to be considered in the flamelet tabulation to improve the overall model fidelity. For tabulation, the user can choose from physical space models, which represent canonical flame configurations subject to some of the aforementioned effects, or composition space models, which have been obtained by a mathematical transformation of the transport equations of species, temperature or enthalpy. However, these models do not necessarily cover the full parameter range or relevant scales which are to be expected in the combustion simulation. For instance, physical space flame configurations are inherently unstable at negative strain conditions (e.g. the rearward stagnation flame [4]). Furthermore, canonical curved flames, such as tubular flames [5], can only cover a limited curvature range due to geometrical restrictions (e.g. minimum realizable nozzle radius). On the contrary, it was shown for turbulent combustion that multi-dimensional flame configurations can experience a much wider range of stretch conditions, including substantial negative strain effects and large curvatures [6].

This serves as the motivation for this work where premixed flame structures are analyzed for a wide range of flame stretch conditions. Flames with effective Lewis numbers smaller and greater than unity are considered. Three physical space models for canonical flame configurations (stagnation flame, spherical expanding flame and inwardly propagating flame) and a recently published composition space model (CSM) [7, 8] are utilized. For the latter, the representation of the flame structure is detached from a specific physical space flame configuration. In our previous work we showed that, when an additional equation for the progress variable gradient is being solved, arbitrary combinations of strain (K_s) and curvature (κ) can be prescribed as external parameters. Setting both parameters to zero, the CSM recovers the unstretched laminar burning velocity s_u^0. Here it is shown that the CSM can access a larger (K_s, κ)-parameter space exceeding the capabilities of canonical flame models, and that this can lead to significant differences for flame structures.

First, the required theory of flame stretch, the CSM, and the canonical flame models is briefly revisited. Then, different flame structures obtained for the canonical flame configurations are discussed and compared. Thereafter, composition space flame solutions are analyzed in the (K_s, κ)-region beyond the limits of canonical flame models. The paper ends with a summary.

2. Flame stretch effects

Flame stretch influences the structure and burning rate of a premixed flame and can lead to flame extinction if increased above a critical value. It is defined as the fractional area change of a flame surface element [9, 10]

$$K = \frac{1}{A}\frac{\mathrm{d}A}{\mathrm{d}t} = \nabla_t \cdot \mathbf{u}_t + (\mathbf{s}_f \cdot \mathbf{n})(\nabla \cdot \mathbf{n}), \tag{1}$$

where $\nabla_t \cdot \mathbf{u}_t$ represents flame-tangential straining by the flow, $\mathbf{s}_f$ is the flame speed, and $\mathbf{n}$ is the flame-normal unit vector ($\mathbf{n}$ points towards the burnt gases). Introducing the decomposition of the flame speed into flow velocity and flame displacement speed, $\mathbf{s}_f = \mathbf{u} - s_d\,\mathbf{n}$, Eq. 1 can be reformulated [11]

$$K = \underbrace{\nabla_t \cdot \mathbf{u}_t - (\mathbf{u} \cdot \mathbf{n})\,\kappa}_{K_s} + \underbrace{s_d\,\kappa}_{K_c}, \tag{2}$$

where $\kappa = -\nabla \cdot \mathbf{n}$ is the flame curvature, K_s marks strain imposed on the flame by the flow, and K_c is a stretch component which originates from the self-propagation of the (curved) flame. This distinction is of importance here since the CSM presented in the next section requires K_s and the flow topology information κ as external parameters. On the contrary, K_c is tied to the flame displacement speed, which is obtained as a flame-response to the external flame parameters. The Markstein length $\mathcal{L}$ is often used to describe the relation between burning velocity s_u and stretch [12]

$$s_u = s_u^0 - \mathcal{L}\,K + H.O.T. \tag{3}$$

Its dimensionless form is denoted as Markstein number $\mathcal{M} = \mathcal{L}/l_f$ with the flame thickness l_f. However, the linear relation is limited to weakly stretched flames and higher order terms ($H.O.T$) gain importance with increasing stretch.

3. Composition space model (CSM)

For a premixed flame, the reaction progress variable Y_c can be utilized as a flame-attached coordinate which spans the so-called progress variable space. Here, it is defined as a weighted sum of species, $Y_c = \sum_i^{n_s} \alpha_i Y_i$. With this, a transport equation for Y_c can be formulated

$$\rho \frac{\partial Y_c}{\partial t} + \rho \mathbf{u} \cdot \nabla Y_c = -\nabla \cdot (\rho Y_c \mathbf{V}_c) + \dot{\omega}_c \,, \tag{4}$$

where ρ is the density and $Y_c \mathbf{V}_c = \sum_i^{n_s} \alpha_i Y_i \mathbf{V}_i$ the diffusive flux of the progress variable, with $\mathbf{V}_i$ being the diffusion velocity of species i. Further, the source term is defined as a weighted sum of species source terms $\dot{\omega}_c = \sum_i^{n_s} \alpha_i \dot{\omega}_i$. The motion of the flame surface, represented by a collection of Y_c-isosurfaces, is then described by the kinematic condition [1, 13]

$$\frac{\mathrm{d}Y_c}{\mathrm{d}t} = \frac{\partial Y_c}{\partial t} + \mathbf{s}_f \cdot \nabla Y_c = 0 \,, \tag{5}$$

and the unit vector along the flame-normal is defined as $\mathbf{n} = \nabla Y_c / |\nabla Y_c|$. The temperature and species balance equations can be transformed into Y_c-space given a suitable choice for the progress variable. Furthermore, an equation for the progress variable gradient $g_c = |\nabla Y_c|$ is required as a closure [7]. The final set of equations reads [8]

$$\begin{aligned} \rho \frac{\partial Y_i}{\partial \tau} &= -g_c \frac{\partial}{\partial Y_c} \left(g_c \rho Y_i \tilde{V}_i \right) + g_c \frac{\partial}{\partial Y_c} \left(g_c \rho Y_c \tilde{V}_c \right) \frac{\partial Y_i}{\partial Y_c} \\ &\quad + \rho g_c \kappa \left(Y_i \tilde{V}_i - Y_c \tilde{V}_c \frac{\partial Y_i}{\partial Y_c} \right) - \dot{\omega}_c \frac{\partial Y_i}{\partial Y_c} + \dot{\omega}_i \,, \end{aligned} \tag{6}$$

$$\begin{aligned} \rho \frac{\partial T}{\partial \tau} &= \frac{g_c}{c_p} \frac{\partial}{\partial Y_c} \left(g_c \lambda \frac{\partial T}{\partial Y_c} \right) + g_c \frac{\partial}{\partial Y_c} \left(g_c \rho Y_c \tilde{V}_c \right) \frac{\partial T}{\partial Y_c} \\ &\quad - \rho g_c^2 \sum_k^{n_s} \frac{c_{p,k}}{c_p} Y_k \tilde{V}_k \frac{\partial T}{\partial Y_c} - \rho g_c \kappa \left(\frac{\lambda}{\rho c_p} + Y_c \tilde{V}_c \right) \frac{\partial T}{\partial Y_c} \\ &\quad - \dot{\omega}_c \frac{\partial T}{\partial Y_c} + \frac{\dot{\omega}_T}{c_p} \,, \end{aligned} \tag{7}$$

$$\begin{aligned} 0 &= -g_c^2 \frac{\partial^2}{\partial {Y_c}^2} \left(g_c \rho Y_c \tilde{V}_c \right) + g_c^2 \frac{\partial}{\partial Y_c} \left(\kappa \rho Y_c \tilde{V}_c \right) \\ &\quad - \dot{\omega}_c \frac{\partial g_c}{\partial Y_c} + g_c \frac{\partial \dot{\omega}_c}{\partial Y_c} + \rho K_s g_c \,, \end{aligned} \tag{8}$$

where $\tilde{V}_i$ represents the diffusion velocity of species i with respect to the Y_c-composition space, λ is the heat conductivity, c_p is the heat capacity and $\dot{\omega}_T$ is the heat release rate. Solutions of these equations recover structure and characteristics of canonical flame configurations, and it has been shown that it is sufficient to approximate the external parameters strain K_s and curvature κ by representative values [8]. Setting strain and curvature to zero, the laminar burning velocity can be computed by solving the closed system of equations [7]. Homogeneous ignition is recovered by the CSM in the asymptotic limit of $g_c \to 0$ [7, 8]. While the CSM can capture transient effects (ignition, flame structure of a spherical flame), it should be noted that it cannot account forvery high transients or cases exhibiting multi-dimensional structures.

4. Canonical premixed flame configurations

Besides the composition space model (CSM), three physical space models for canonical flame configurations are considered which are shown schematically in Fig. 1. Planar stagnation flames (STAG) can be stabilized in a stream of premixed fresh gases towards a wall or an opposed stream of equivalent composition (twin-configuration). The governing equations can be found in Kee et al. [14]. In a quiescent mixture of fresh gases, a spherical expanding flame (SEF) can be created using an ignition source. This flame is stretched and curved at the same time and both quantities change as the flame evolves over time. Unlike SEF, an inwardly propagating flame (IPF) is obtained by igniting a quiescent mixture of fresh gases in perfect spherical shape. The flame then propagates inwards consuming the remaining fresh gases. Although such an idealized flame can hardly be established in experiments, it can be computed numerically [15, 16]. Both spherical flames are computed using the code A-SURF [17]. Table 1 summarizes the stretch conditions for all three configurations.

5. Results

With the possibility to choose arbitrary combinations of strain and curvature, the CSM allows studying the influence of K_s and κ on premixed flame structures systematically, which is the objective in the following. By contrast, strain and curvature are inherently determined through the boundary conditions and configuration for the canonical flames. Exemplary canonical flame solutions are analyzed and compared against the CSM in the (K_s, κ)-parameter space. As an estimate for the parameter variation, Fru et al. [6] found strain and curvature in the order of $K_s \approx \pm 10^4\,\mathrm{s}^{-1}$ and $\kappa \approx \pm 10^4\,\mathrm{m}^{-1}$ from direct numerical simulations of turbulent premixed flames in a periodic box. Although different values might be found in other multi-dimensional flame configurations, these orders of magnitude serve as an orientation here. After comparing the CSM against canonical flame solutions, flame structures beyond the limit of canonical flames are analyzed. Flame databases for two different fuels are created: (1) lean hydrogen/air flames ($\phi = 0.5$, $Le_{\mathrm{H_2}} \approx 0.3$, $\approx$ 12000 flame calculations) and (2) lean ethanol flames ($\phi = 0.7$, $Le_{\mathrm{C_2H_5OH}} \approx 1.6$, $\approx$ 6000 flame calculations). For the flames specified above, the fuel

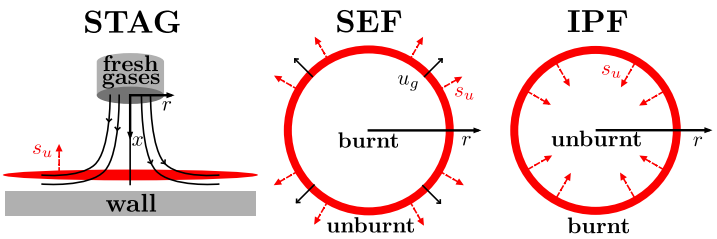

Fig. 1: Schematic models of the canonical flame configurations considered.

Tab. 1: Overview of stretch effects in the canonical flames considered.

Type	stretch $K = K_s + K_c$	strain K_s	curvature stretch K_c
STAG	$K > 0$	$K_s > 0$	$K_c = 0$
SEF	$K > 0$	$K_s > 0$	$K_c > 0$
IPF	$K < 0$	$K_s = 0$	$K_c < 0$

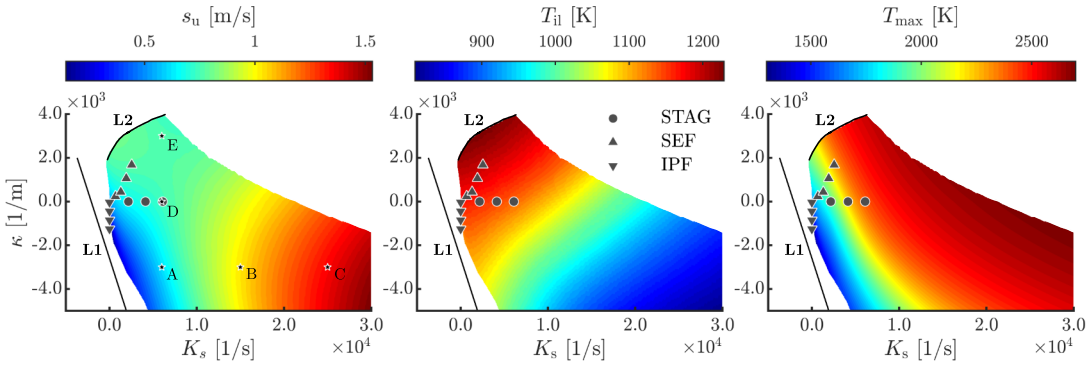

Fig. 2: (K_s, κ)-parameter space for lean H_2/air flames ($\phi = 0.5$, $p = 1$ atm, $T_0 = 300$ K) characterized by burning velocity s_u (left), inner layer temperature T_{il} (middle) and maximum temperature T_{max} (right). Canonical flame solutions are shown for reference. Furthermore, limits of the parameter space are indicated (L1: Strain-induced extinction limit, L2: Topological limit).

is the deficient reactant and its Lewis number is considered the effective Lewis number [18]. The applied progress variable definitions are $Y_c = Y_{H_2O} - Y_{H_2} - Y_{O_2}$ for hydrogen and $Y_c = Y_{H_2O} - Y_{O_2} + Y_{CO_2} + 10\,Y_{H_2}$ for ethanol flames. A mixture averaged diffusion model is utilized [19] and thermal diffusion [20] is additionally considered for hydrogen-air flames.

5.1. Le < 1 *flames* (H_2)

Figure 2 shows the characteristics of lean H_2-air flames in the (K_s, κ)-parameter space obtained with the CSM. Reference solutions of canonical flames are included in the figure and it is observed that they only cover a small subset of the parameter range accessible by the composition space solutions. The plot on the left shows the burning velocity s_u. It is evaluated at the maximum heat release peak, which is in agreement with literature as it should be evaluated close to the burned side [11, 12] and is weighted by the fresh gas density ρ^0, according to

$$s_u = \frac{\rho s_d}{\rho^0} = \frac{1}{\rho^0}\left(-\frac{\partial}{\partial Y_c}\left(\rho Y_c \tilde{V}_c\right) + \kappa \rho Y_c \tilde{V}_c + \frac{\dot{\omega}_c}{g_c}\right). \quad (9)$$

This equation can be obtained using the transformed Eqs. (4) and (5) [8]. Furthermore, Fig. 2 shows the inner layer temperature T_{il}, which is the temperature at the maximum heat release rate (middle), and the maximum temperature T_{max} (right). Moreover, the limits of the parameter space are indicated, as discussed further below.

Positive strain strengthens Le < 1 flames due to differential diffusion [18], as reflected in Fig. 2 illustrating that the burning velocity increases by a factor of approximately 5 from the left to the right boundary of the parameter space. Furthermore, the maximum temperature increases substantially with increasing K_s. The influence of strain on the flame structure is more significant than the effect resulting from curvature. This is also observed for the burning velocity, whereas the maximum temperature shows a moderate effect. On the other hand, both strain and curvature influence the inner layer temperature. T_{il} increases with increasing strain (decreasing curvature), which indicates that the heat release peak is shifted to lower (higher) temperatures, respectively.

Exemplary flame structures of canonical flame configurations are compared to corresponding results from the CSM in Fig. 3. Temperature, fuel and OH mass fractions are shown as a function of the progress variable. Overall, good agreement is observed between the canonical flame solutions and the CSM. Slight deviations occur at the right boundary for STAG flames resulting from restrainment effects which are discussed further below. For the SEF, small discrepancies can be observed in the hydrogen profile. These result from using representative values for strain and curvature in the

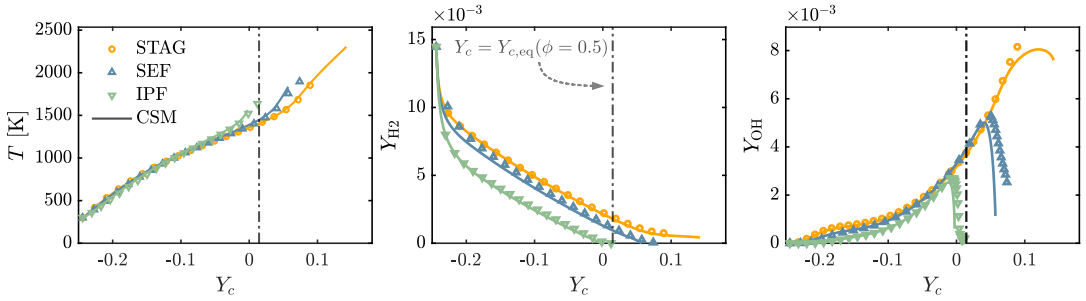

Fig. 3: Flame structure for lean H_2-air flames ($\phi = 0.5$, $p = 1$ atm, $T_0 = 300$ K) of canonical flames (symbols) compared to calculations with the CSM (lines). (STAG: $K_s = 4800\,\mathrm{s}^{-1}$ and $\kappa_c = 0\,\mathrm{m}^{-1}$, SEF: $K_s = 900\,\mathrm{s}^{-1}$ and $\kappa_c = 310\,\mathrm{m}^{-1}$, IPF: $K_s = 0\,\mathrm{s}^{-1}$ and $\kappa_c = -280\,\mathrm{m}^{-1}$).

CSM, and these are extracted at the maximum heat release peak for both spherical flames, while they vary in the physical space (SEF/IPF model). Nevertheless, the CSM can recover the flame structure of the SEF for an instant during its transient evolution [8]. The larger progress variable domain for the SEF is a direct consequence of the ignition process, which produces already burned products and a developed radical pool [21]. The flame structures of the IPF are captured well by the CSM. IPF solutions for large negative curvatures could not be matched by corresponding composition space solutions, presumably due to the fact that IPFs are weakly back-supported by hot products while propagating inwardly. This effect is not included in the CSM.

Restrainment of stagnation flames. Although lean H_2-flames (Le < 1) are strengthened by positive strain, the corresponding STAG flames exhibit a positive strain extinction limit. According to Law [18], this extinction behavior is due to *restrainment* of the flame and not a stretch effect. Increasing the strain rate, extinction of STAG flames does not occur before the flame reaches the (adiabatic) stagnation plane. At the stagnation plane the flame is restrained, i.e. it cannot occupy enough space (limited flame thickness) and the residence times of reactants and intermediates are reduced. When the strain is further increased, chemical reactions remain incomplete and eventually the flame is extinguished. Restrainment is specific to the physical space STAG flame configuration. Such limitations are avoided in composition space. Instead, the CSM is defined such that both boundary conditions (fresh and burned gases) are far away from the reaction zone. This is readily understood from the boundary conditions for the gradient ($g_c = 0$), which represents the transformation between Y_c and coordinate $\mathrm{d}x = \mathrm{d}Y_c/g_c$ measured along the flame-normal in the physical space.

For further illustration, Fig. 4 shows STAG solutions subject to restrainment at elevated strain rates K_s and corresponding composition space solutions (unrestrained). Inner layer quantities, such as T_{il}, remain unaffected by restrainment until extinction of the STAG flames. On the contrary, the maximum temperature is affected as $T_{\max}$ is reached in the post-oxidation zone, which becomes restrained at the stagnation plane.

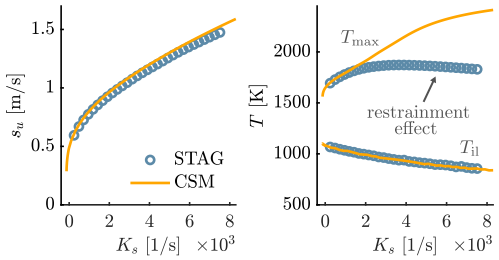

Fig. 4: Restrainment effect for premixed H_2-air STAG flames ($\phi = 0.5$, $p = 1$ atm, $T_0 = 300$ K) compared to the CSM.

Flame structure analysis in composition space. In Fig. 5 the temperature T, the local equivalence ratio ϕ_{local} and the heat release rate $\dot{\omega}_T$ are shown in composition space for three different cases with constant curvature and increasing strain from case A to C, respectively. The maximum of the progress variable increases with increasing strain indicating super equilibrium conditions ("hot spots") which have been identified for laminar and turbulent flames [22, 23]. This is further affirmed by the maximum heat release peak and the increased local equivalence ratio, which both increase with K_s. Note that the integral of the heat release across the flame remains constant, the flame only becomes thinner and the gradient g_c assumes larger values (not shown).

Figure 6 shows the complementary result to Fig. 5. Here, the strain rate is fixed, while the curvature is varied. In accordance with the literature [18], the figure shows that positive curvature strengthens the flame, while negative curvature has the opposite effect. Interestingly, particularly the flame structure for case C can only be realized with the CSM, utilizing a compensation

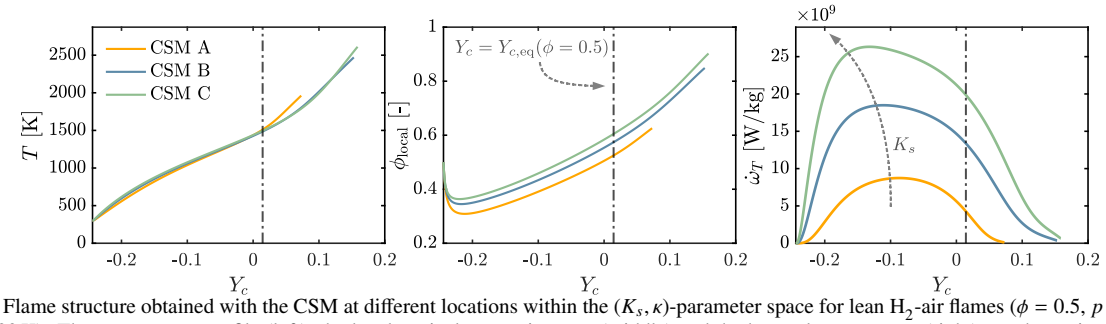

Fig. 5: Flame structure obtained with the CSM at different locations within the (K_s, κ)-parameter space for lean H_2-air flames ($\phi = 0.5$, $p = 1$ atm, $T_0 = 300$ K). The temperature profile (left), the local equivalence ratio ϕ_{local} (middle) and the heat release rate $\dot{\omega}_T$ (right) are shown in Y_c-space. The curvature is fixed at $\kappa = -3000\,\mathrm{m}^{-1}$ while strain K_s is increased for cases A/B/C according to $6000/15000/25000\mathrm{s}^{-1}$.

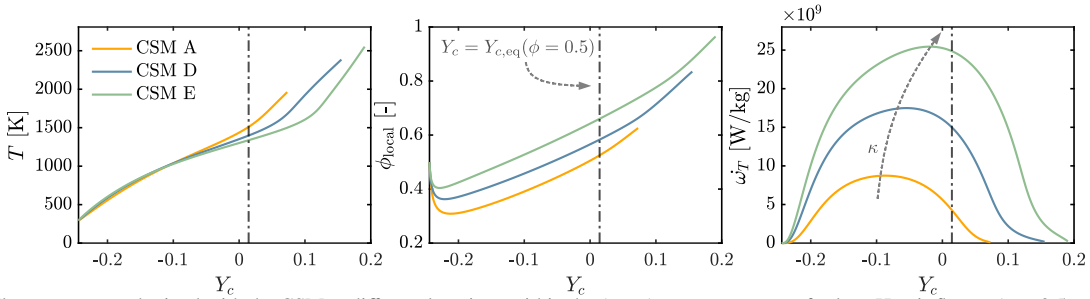

Fig. 6: Flame structure obtained with the CSM at different locations within the (K_s, κ)-parameter space for lean H_2-air flames ($\phi = 0.5$, $p = 1$ atm, $T_0 = 300$ K). The temperature profile (left), the local equivalence ratio ϕ_{local} (middle) and the heat release rate $\dot{\omega}_T$ (right) are shown as a function of Y_c. Strain is fixed at $K_s = 6000\,\mathrm{s}^{-1}$ while curvature κ is increased for cases A/D/E according to $-3000/0/3000\mathrm{m}^{-1}$.

between opposing trends for positive strain and negative curvature effects. It is also found that the maximum heat release peak shifts towards fresh gases with increasing strain, while the opposite is true for increasing curvature.

Limits in strain-curvature parameter space. It is indicated in Fig. 2 that the composition space solutions exhibit certain limits in the (K_s, κ)-parameter space. These limits originate from considerations about flame physics as outlined in the following.

L1: Strain-induced extinction limit. Le < 1 flames are strengthened (weakened) by positive (negative) strain and vice versa for flames with Le > 1 [18]. Hence, strain can weaken a flame such that heat release rate and burning velocity become significantly reduced up to a point where the flame quenches. This strain-induced extinction limit L1 is estimated in (K_s, κ)-space by extrapolating the burning velocity to zero.

L2: Topological limit. The CSM assumes that the flame structure is locally one-dimensional. However, considering a flame whose flame thickness is of the order of the curvature length scale (i.e. the flame radius, $l_\kappa = 1/\kappa$) implies a flame kernel structure rather than a flame surface. Solutions in the limit of the flame kernel structure require separate analyses and modeling, which is out of scope for this work. Therefore, a topological limit is introduced which restricts the flame thickness

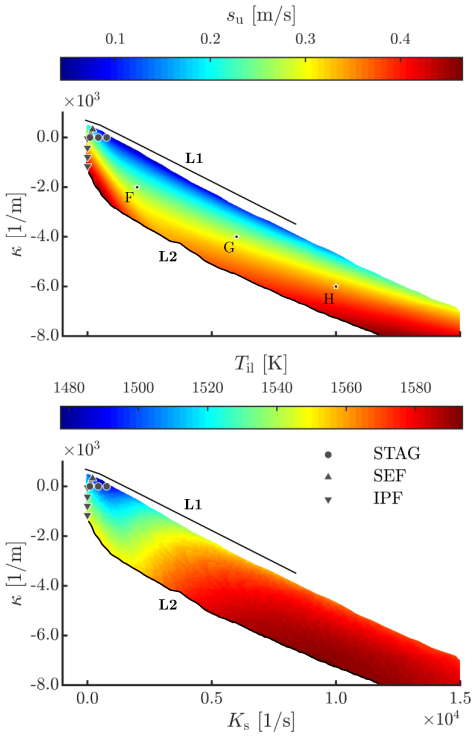

Fig. 7: (K_s, κ)-parameter space for lean C_2H_5OH/air flames ($\phi = 0.7$, $p = 1$ atm, $T_0 = 363$ K) characterized by burning velocity s_u (top) and inner layer temperature T_{il} (bottom). Further, canonical flame solutions and the respective limits (L1: Strain-induced extinction limit, L2: Topological limit) are shown.

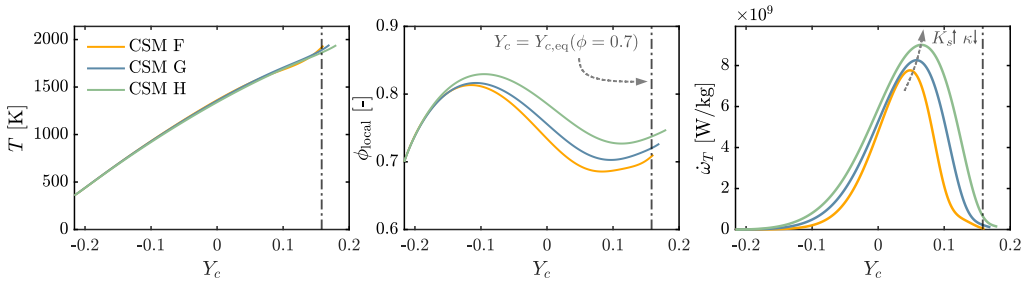

Fig. 8: Flame structure obtained with the CSM at different locations within the (K_s, κ)-parameter space of lean C_2H_5OH-air flames ($\phi = 0.7$, $p = 1$ atm, $T_0 = 363$ K). The temperature profile (left), the local equivalence ratio ϕ_{local} (middle) and the heat release rate $\dot{\omega}_T$ (right) are shown for three different cases as a function of Y_c (Case F: $K_s = 2000\,\mathrm{s}^{-1}$, $\kappa_c = -2000\,\mathrm{m}^{-1}$, Case G: $K_s = 6000\,\mathrm{s}^{-1}$, $\kappa_c = -4000\,\mathrm{m}^{-1}$, Case H: $K_s = 10000\,\mathrm{s}^{-1}$, $\kappa_c = -6000\,\mathrm{m}^{-1}$)

to be smaller than the curvature length scale by at least a factor of 3, $l_f < l_\kappa/3$. For this criterion the Zeldovich thickness is utilized $l_f = \lambda/(c_p \rho_u s_u)$ instead of a thickness definition based on the progress variable gradient, as this would introduce numerical uncertainties due to reconstruction of the physical space coordinate.

5.2. Le > 1 *flames* (C_2H_5OH)

Figure 7 shows the burning velocity (top) and inner layer temperature (bottom) for lean C_2H_5OH/air flames. The (K_s, κ)-parameter space attainable with the CSM is smaller and shaped differently than for H_2-air flames. There is only a small area with positive strain and positive curvature for ethanol flames and the strain induced extinction limit is found for positive strain. This is in agreement with theory [18] since Le > 1 flames are weakened by positive stretch. The burning velocity s_u increases by a factor of 4 and T_{il} increases by approximately 100 K for increasing strain and decreasing curvature. The variations of maximum temperature (not shown) are comparable to the ones for T_{il}, with a slight decrease towards the upper boundary.

Similarly as for H_2-air flames, the CSM recovers the canonical flame structures for C_2H_5OH-air flames (not shown here, cf. [8]). Figure 8 shows temperature T, local equivalence ratio ϕ_{local} and the heat release rate $\dot{\omega}_T$ obtained for C_2H_5OH-air flames with the CSM from parameter variation (cases F-H, as indicated in Fig. 7). For Cases F to H, curvature decreases and strain rate increases. The maximum local equivalence ratio and the maximum heat release peak increases from F to H, which is expected for Le > 1 flames. On the other hand, the temperature profiles are almost identical and the shift of the maximum heat release peak is smaller compared to hydrogen. This underlines that stretch effects are less pronounced for C_2H_5OH-air flames, however, particularly the effects on s_u are significant (cf. Fig. 7).

5.3. *Markstein numbers*

Usually the Markstein length is obtained via a regression of burning velocity versus stretch [12]. In the (K_s, κ)-parameter space the Markstein length can be evaluated as the directional derivative of the burning velocity with respect to stretch $\mathcal{L} = \partial s_u/\partial K = \nabla s_u \cdot \nabla K/|\nabla K|^2$. Fig. 9 shows the Markstein number for the whole parameter space. The Markstein number changes only slightly in the region of the canonical flames. This is in agreement with theory, since the Markstein number can be assumed constant for weakly stretched flames [11, 12]. The Markstein number decreases towards the strain induced extinction limit as the burning velocity rapidly approaches zero. Overall, it is observed that the Markstein number changes significantly with respect to both, K_s and κ.

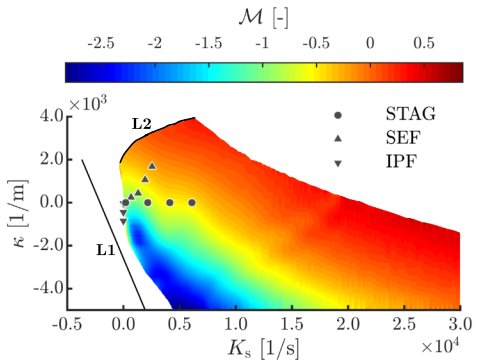

Fig. 9: Markstein number for lean H_2-air flames ($\phi = 0.5$, $p = 1$ atm, $T_0 = 300$ K) in the (K_s, κ)-parameter space.

6. Summary and conclusions

In this work, stretch effects on premixed flame structures are investigated for flames with effective Lewis numbers smaller (lean H_2-air) and larger than unity (lean C_2H_5OH-air). Three canonical flame configurations (expressed and solved with respect to the physical space) and a recently published composition space model (CSM) are considered. The latter describes premixed flame structures in progress variable space and allows arbitrary combinations of strain and curvature to be chosen. By this means, the CSM recovers the canonical flame structures with one set of equations, while different models have to be used when computing the

same flame structures in the physical space. Moreover, a larger region in the strain-curvature parameter space becomes attainable with the CSM. This has several reasons: (1) strain and curvature are inherently prescribed through boundary conditions for canonical flame configurations, and (2) canonical flame configurations are subject to certain limitations (e.g. with respect to the burner geometry, restrainment of stagnation flames).

The flame structure analysis for the lean H_2-air flames shows that strain effects can lead to burning velocities which differ by a factor of more than 5 and substantially different flame temperatures for the same thermochemical state of the fresh gases. For lean C_2H_5OH-air flames, the variability of these flame characteristics is smaller, but also significant. The evaluation of the Markstein number for hydrogen flames shows that this quantity changes only slightly in the region of the canonical flames, whereas significant changes are observed for higher strain and curvature.

It is noted, that canonical flames can only represent a small part of the strain-curvature parameter space and therefore only capture a certain portion of stretch effects on premixed flame structures. This could become relevant for multi-dimensional flame modeling in the context of tabulated chemistry approaches. These methods often rely on canonical flame solutions for the construction of look-up tables especially considering the significant changes of key quantities (such as the burning velocity) with strain and curvature. Hence, these modeling strategies could benefit from the CSM discussed here, incorporating a wider variability of stretch effects on premixed flame structures.

Acknowledgments

Financial support is kindly acknowledged from the German Research Foundation (DFG) - Project No. 411275182 and the National Natural Science Foundation of China - Project No. 51861135309.

References

[1] J. A. van Oijen, A. Donini, R. J. M. Bastiaans, J. H. M. ten Thije Boonkkamp, L. P. H. de Goey, *State-of-the-art in premixed combustion modeling using flamelet generated manifolds*, Prog. Energy Combust. Sci. 57 (2016) 30 – 74.

[2] O. Gicquel, N. Darabiha, D. Thévenin, *Laminar premixed hydrogen/air counterflow flame simulations using flame prolongation of ILDM with differential diffusion*, Proc. Combust. Inst. 28 (2000) 1901 – 1908.

[3] N. Peters, *Laminar Flamelet Concepts in Turbulent Combustion*, Symp. (Int.) Combust. 21 (1988) 1231–1250.

[4] C. Law, C. Sung, *Structure, aerodynamics, and geometry of premixed flamelets*, Prog. Energy Combust. Sci. 26 (2000) 459 – 505.

[5] R. W. Pitz, S. Hu, P. Wang, *Tubular premixed and diffusion flames: Effect of stretch and curvature*, Prog. Energy Combust. Sci. 42 (2014) 1 – 34.

[6] G. Fru, G. Janiga, D. Thévenin, *Impact of Volume Viscosity on the Structure of Turbulent Premixed Flames in the Thin Reaction Zone Regime*, Flow Turbul. Combust. 88 (2012) 451–478.

[7] A. Scholtissek, P. Domingo, L. Vervisch, C. Hasse, *A self-contained progress variable space solution method for thermochemical variables and flame speed in freely-propagating premixed flamelets*, Proc. Combust. Inst. 37 (2018) 1529–1536.

[8] A. Scholtissek, P. Domingo, L. Vervisch, C. Hasse, *A self-contained composition space solution method for strained and curved premixed flamelets*, Combust. Flame 207 (2019) 342–355.

[9] F. A. Williams, *A review of some theoretical considerations of turbulent flame structure*, AGARD Conference Proceeding, 1975 (1975).

[10] S. Chung, C. Law, *An invariant derivation of flame stretch*, Combust. Flame 55 (1984) 123 – 125.

[11] G. R. A. Groot, J. A. van Oijen, L. P. H. de Goey, K. Seshadri, N. Peters, *The effects of strain and curvature on the mass burning rate of premixed laminar flames*, Combust. Theor. Model. 6 (2002) 675–695.

[12] G. K. Giannakopoulos, A. Gatzoulis, C. E. Frouzakis, M. Matalon, A. G. Tomboulides, *Consistent definitions of "Flame Displacement Speed" and "Markstein Length" for premixed flame propagation*, Combust. Flame 162 (2015) 1249 – 1264.

[13] M. Matalon, *On Flame Stretch*, Combust. Sci. Technol. 31 (1983) 169–181.

[14] R. J. Kee, J. A. Miller, G. H. Evans, G. Dixon-Lewis, *A computational model of the structure and extinction of strained, opposed flow, premixed methane-air flames*, Symp. (Int.) Combust. 22 (1989) 1479 – 1494.

[15] D. Bradley, P. H. Gaskell, X. J. Gu, *Burning velocities, markstein lengths, and flame quenching for spherical methane-air flames: A computational study*, Combust. Flame 104 (1996) 176–198.

[16] Z. Chen, X. Gou, Y. Ju, *Studies on the Outwardly and Inwardly Propagating Spherical Flames with Radiative Loss*, Combust. Sci. Technol. 182 (2010) 124–142.

[17] Z. Chen, X. Qin, Y. Ju, Z. Zhao, M. Chaos, F. L. Dryer, *High temperature ignition and combustion enhancement by dimethyl ether addition to methane–air mixtures*, Proc. Combust. Inst. 31 (2007) 1215–1222.

[18] C. K. Law, Combustion Physics, Cambridge University Press (CUP), 2006.

[19] C. F. Curtiss, J. O. Hirschfelder, *Transport Properties of Multicomponent Gas Mixtures*, The Journal of Chemical Physics 17 (1949) 550–555.

[20] A. Ern, V. Giovangigli, Multicomponent Transport Algorithms, Springer Berlin Heidelberg, 1994.

[21] Y. Wang, W. Han, Z. Chen, *Effects of fuel stratification on ignition kernel development and minimum ignition energy of n-decane/air mixtures*, Proc. Combust. Inst. 37 (2019) 1623 – 1630.

[22] A. J. Aspden, M. S. Day, J. B. Bell, *Turbulence-flame interactions in lean premixed hydrogen: transition to the distributed burning regime*, J. Fluid Mech. 680 (2011) 287–320.

[23] J. Schlup, G. Blanquart, *Reproducing curvature effects due to differential diffusion in tabulated chemistry for premixed flames*, Proc. Combust. Inst. (2018).